




 Cite this: *Phys. Chem. Chem. Phys.*, 2022, 24, 13149

Infrared spectroscopy of $\text{Be}(\text{CO}_2)_4^+$ in the gas phase: electron transfer and C–C coupling of CO_2^\ddagger

 Yang Yang, Yangyu Zhou, Xiaoyang Jin, Guanjun Wang  and Mingfei Zhou *

Beryllium–carbon dioxide cation complexes $\text{Be}(\text{CO}_2)_n^+$ are produced by a laser vaporization-supersonic expansion ion source in the gas phase. Mass-selected infrared photodissociation spectroscopy supplemented by theoretical calculations confirms that $\text{Be}(\text{CO}_2)_4^+$ is a coordination saturated complex that can be assigned to a mixture of two isomers. The first structure involves a bent CO_2^- ligand that is bound in a monodentate $\eta^1\text{-O}$ coordination mode. Another isomer has a metal oxalate-type C_2O_4^- moiety with a C–C hemibond.

 Received 19th April 2022,
 Accepted 14th May 2022

DOI: 10.1039/d2cp01788a

rsc.li/pccp

Introduction

The fixation and transformation of carbon dioxide, a naturally abundant carbon source that contributes to the greenhouse effect, into useful chemicals are receiving increased attention.^{1,2} The coordination of carbon dioxide to a metal center is proposed to be the initial step of catalytic activation of carbon dioxide.³ Previous experimental and theoretical studies have shown that carbon dioxide can bind to the metal centers in various coordination modes.^{4–6} The manner by which carbon dioxide binds to the metal centers is an important factor to influence the extent of activation and subsequent transformation.

The coordination of carbon dioxide by neutral metal atoms and molecular metal oxide species has been investigated spectroscopically in cryogenic matrices.^{7–11} Various carbon dioxide complexes in monodentate ($\eta^1\text{-C}$) and bidentate ($\eta^2\text{-C, O}$ and $\eta^2\text{-O, O}$) coordination modes were formed and identified spectroscopically.^{7–11} In these complexes, the CO_2 ligands possess a bent structure resulting from the transfer of electron density from the metal centers. Such complexes constitute the first intermediates in the reductive activation of carbon dioxide, which can be photoisomerized to the inserted oxocarbonyl species for some metal systems.^{8–11}

Besides the neutral complexes, some charged metal–carbon dioxide complexes have also been studied by infrared photodissociation spectroscopy in the gas phase. It was found that both the monodentate and bidentate coordination modes are

quite common in anionic metal– CO_2 complexes.^{12–18} For instance, the monodentate $\eta^1\text{-C}$ coordination mode has been identified in the $[\text{MCO}_2]^-$ complexes with $\text{M} = \text{Cu, Ag, Au}$ and Bi .^{12–15} The higher coordinated complexes $[\text{M}(\text{CO}_2)_n]^-$ with $n \geq 2$ for $\text{M} = \text{Co}$ and Ni were characterized to involve a core ion composed of two CO_2 ligands both of which are bound to the metal center in a bidentate $\eta^2\text{-C, O}$ manner.^{16,17} The bidentate $\eta^2\text{-O, O}$ coordination mode was identified in the $[\text{ClMgCO}_2]^-$ complex.¹⁹ In addition, the reduction of carbon dioxide in forming the metal–oxalate species with a covalent C–C bond has been observed in the alkali metal as well as bismuth complexes $[\text{M}(\text{CO}_2)_n]^-$ ($\text{M} = \text{alkali metal, Bi}$).^{15,20}

The CO_2 ligand is bound to the metal center exclusively in an end-on $\eta^1\text{-O}$ fashion in the cationic complexes.^{21–35} The binding between the metal cation and carbon dioxide is largely an electrostatic interaction, resulting in a blue-shifted antisymmetric CO_2 stretching vibration with respect to the free CO_2 molecule.^{21–35} Solvation-induced metal cation \rightarrow carbon dioxide electron transfer with the formation of a bent CO_2^- moiety was reported on the $\text{Mg}(\text{H}_2\text{O})_n(\text{CO}_2)^+$ complexes with $n \geq 3$.²⁷ Metal cation \rightarrow ligand electron transfer reaction in forming an oxalate-type C_2O_4^- anion species was proposed in the $\text{V}(\text{CO}_2)_n^+$ $n \geq 7$ clusters,²⁸ which was later reassigned to a charge transfer complex involving a bidentate $\eta^2\text{-C, O}$ coordinated CO_2^- ligand.³³ Solvation-induced intracluster insertion reaction producing the oxocarbonyl species has also been reported in the larger $[\text{M}(\text{CO}_2)_n]^+$ complexes with $\text{M} = \text{Ti, Ni, Si}$ and $n \geq 5$.^{24–26} Recent investigation on the end-on $\eta^1\text{-O}$ coordinated $[\text{BeOCO}]^+$ complex in solid neon matrix indicates that the bonding between the metal cation and CO_2 exhibits significant covalent character due to the interference of the wave function.³⁶ Here we report the generation and infrared spectroscopic characterization of the larger $\text{Be}(\text{CO}_2)_n^+$ complexes in the gas phase,

Department of Chemistry, Shanghai Key Laboratory of Molecular Catalysts and Innovative Materials, Fudan University, Shanghai 200438, China.
 E-mail: mfzhou@fudan.edu.cn

† Electronic supplementary information (ESI) available. See DOI: <https://doi.org/10.1039/d2cp01788a>

revealing the formation of electron transfer and C–C coupled species.

Experimental and theoretical methods

The cation complexes were generated in the gas phase using a pulsed laser vaporization/supersonic expansion ion source and were studied by infrared photodissociation spectroscopy as described in detail previously.³⁷ The 1064 nm fundamental of a Nd:YAG laser (Continuum, Minilite II) with 10–20 mJ pulse⁻¹ was employed to ablate a beryllium metal target. The cation complexes were produced from the laser vaporization process in expansions of helium seeded with 5% CO₂ using a pulsed valve (General Valve, Series 9) at 0.6–1.2 MPa backing pressure. After free expansion, the cations were skimmed and analyzed by a time-of-flight mass spectrometer. The species of interest were mass-selected and decelerated before being subjected to infrared photodissociation by a tunable IR laser generated *via* an OPO/OPA system (Laser Vision) pumped by a Nd:YAG laser (Continuum Surelite EX). The fragment ions together with the undissociated parent ions were reaccelerated and detected by a second collinear time-of-flight mass spectrometer. IR spectra were recorded by monitoring the relative yield of fragment ions as a function of the photodissociation IR laser wavelength. The spectra were recorded by scanning the dissociation laser in steps of 2 cm⁻¹ and averaging over 300 laser shots at each wavenumber.

Quantum chemical calculations were performed on the Be(CO₂)_n⁺ (*n* = 1–5) complexes. The stochastic surface walking (SSW) global optimization method³⁸ was used to search for the possible stable isomers with the large-scale DFT calculations at the B3LYP/6-311+G* level.^{39–42} The search started from a few guessed structures and stopped until no further stable structure appeared after extensive runs. The low-lying stable isomers were then re-optimized at the B3LYP-D3/aug-cc-pVTZ level to confirm the relative energy sequence and to benchmark with the experimental IR spectrum.⁴³ Further single-point energy calculations on the optimized structures of the two lowest-lying isomers of Be(CO₂)₄⁺ were carried out at the CCSD(T)/cc-pVTZ level.⁴⁴ All calculations were carried out using the Gaussian 09 program.⁴⁵ Theoretically predicted IR spectra were obtained by applying Lorentzian functions with the theoretical harmonic vibrational frequencies scaled by a factor of 0.975 and a 5 cm⁻¹ full width at half-maximum (fwhm). The scaling factor was obtained from the ratio of the experimental antisymmetric stretching frequency of 2349 cm⁻¹ for CO₂ and the calculated value of 2409 cm⁻¹.

The energy decomposition analysis with the natural orbitals of the chemical valence (EDA-NOCV) method⁴⁶ was employed for the metal–ligand bonding analysis at the BP86/TZ2P level using the B3LYP/aug-cc-pVTZ optimized geometries with the ADF2014 program package.^{47–49} In this analysis, the intrinsic interaction energy (ΔE_{int}) between two fragments can be divided into three energy components as follows: the electrostatic interaction energy (ΔE_{elstat}), the Pauli repulsion (ΔE_{Pauli})

and the orbital interaction energy (ΔE_{orb}). Therefore, the interaction energy (ΔE_{int}) between two fragments can be defined as $\Delta E_{\text{int}} = \Delta E_{\text{elstat}} + \Delta E_{\text{Pauli}} + \Delta E_{\text{orb}}$.

Results and discussion

The mass spectrum of the cation complexes produced by laser vaporization of a beryllium metal target in an expansion of helium seeded with 5% carbon dioxide is shown in Fig. 1. The spectrum mainly consists of two groups of mass peaks that can be assigned to the Be(CO₂)_n⁺ (*n* = 3–5) and Be₂O(CO₂)_n⁺ (*n* = 3, 4) complexes based on the *m/z* ratios. The mass peak of Be(CO₂)₄⁺ is always the most intense peak in the spectrum at different experimental conditions, suggesting that this cation might be a coordinatively saturated complex. The Be(CO₂)_n⁺ (*n* = 4, 5) cation complexes were each mass-selected and subjected to infrared photodissociation. Both complexes were found to be able to dissociate *via* the loss of a neutral CO₂ ligand. The Be(CO₂)₄⁺ cation dissociates only under focused IR laser irradiation with quite low efficiency in the low frequency region (1000–1500 cm⁻¹). In contrast, the Be(CO₂)₅⁺ cation dissociates more efficiently in the low frequency region. The vibrational spectra in the 1000–2500 cm⁻¹ region for the *n* = 4 and 5 complexes are shown in Fig. 2.

Both spectra exhibit strong bands in the 2300–2400 cm⁻¹ frequency region, which can be attributed to the antisymmetric OCO stretching vibrations of the η¹-O coordinated CO₂ ligands. The band of Be(CO₂)₄⁺ in this region is quite broad and cannot be well-resolved. In contrast, well-resolved bands at 2350, 2388 and 2404 cm⁻¹ were observed for the Be(CO₂)₅⁺ complex. The sharp band at 2350 cm⁻¹ for the Be(CO₂)₅⁺ complex is very close to the antisymmetric stretching mode of free CO₂, and is due to the absorption of a weakly bound CO₂ ligand. The spectra in the low frequency region for the *n* = 4 and 5 complexes are quite similar except that the band intensities of the *n* = 4 complex are much weaker than those of the *n* = 5 complex. These experimental observations imply that the *n* = 5 complex is a weakly bound complex involving a Be(CO₂)₄⁺ core cation.

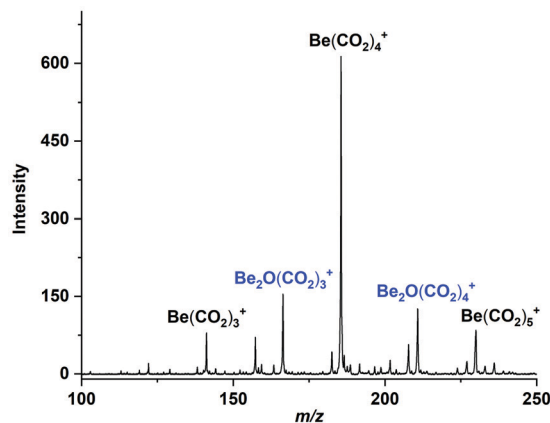


Fig. 1 Mass spectrum of the cation complexes produced by pulsed laser vaporization of a beryllium metal target in an expansion of helium seeded with carbon dioxide.

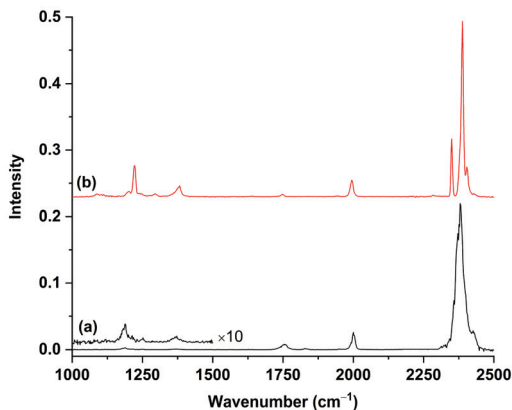


Fig. 2 Infrared photodissociation spectra of (a) $\text{Be}(\text{CO}_2)_4^+$ (in black) and (b) $\text{Be}(\text{CO}_2)_5^+$ (in red).

Quantum chemical calculations were firstly performed on the $\text{Be}(\text{CO}_2)_4^+$ cation complex. Six stable isomers lying within 40 kcal mol^{-1} were found using the stochastic surface walking method. The structures and relative stabilities optimized at the higher B3LYP-D3/aug-cc-pVTZ level are shown in Fig. S1 in the ESI.† The lowest-energy isomer (Fig. 3, **1A**) has a C_2 symmetric structure involving a C_2O_4 moiety and two equivalent η^1 -O end-on coordinated CO_2 ligands. The C_2O_4 unit is coordinated to the beryllium center *via* two O atoms. It has a calculated C–C bond distance of 2.075 \AA , which is close to that of the C_2O_4^- anion (1.985 \AA),^{50,51} but is significantly longer than that in the $\text{C}_2\text{O}_4^{2-}$ dianion (1.574 \AA)⁵¹ calculated at the similar level of theory, suggesting that the **1A** isomer is a metal–oxalate species, $\text{Be}^{2+}(\text{C}_2\text{O}_4^-)(\text{OCO})_2$. The second lowest-lying isomer has C_s symmetry (Fig. 3, **1B**) involving a quite bent CO_2 ligand and three nearly linear η^1 -O end-on coordinated CO_2 ligands. The bent CO_2 ligand has a predicted OCO bond angle of 129.7° , which is slightly more acute than that of the free CO_2^- anion (134°).^{51–54} The **1B** structure can be described as $\text{Be}^{2+}(\text{CO}_2^-)(\text{OCO})_3$. The **1B** isomer is predicted to be about $4.7 \text{ kcal mol}^{-1}$ higher in energy than the most stable structure **1A** at the B3LYP-D3/aug-cc-pVTZ level after zero point energy correction. The energy difference is reduced to be only $1.1 \text{ kcal mol}^{-1}$ at the CCSD(T)/cc-pVTZ//B3LYP-D3/aug-cc-pVTZ level of theory. The third structure **1C** (Fig. S1, ESI†) involves a bidentate η^2 -O, O coordinated CO_2^- ligand and three nearly linear η^1 -O end-on coordinated CO_2 ligands. The fourth structure **1D** (Fig. S1, ESI†) is a carbonate–carbonyl complex with the carbonate unit being bonded to the beryllium center *via* a single O atom. The fifth isomer **1E** (Fig. S1, ESI†) is a weakly bound complex featuring a $\text{Be}(\text{OCO})_3^+$ core ion and a weakly tagged CO_2 O-bound ligand. All of the three CO_2 ligands in the $\text{Be}(\text{OCO})_3^+$ core ion possess the η^1 -O coordination mode. The sixth isomer **1F** (Fig. S1, ESI†) is an inserted oxocarbonyl species coordinated by two nearly linear η^1 -O end-on CO_2 ligands. The last four isomers were predicted to be 13.3 , 29.6 , 33.3 and $37.4 \text{ kcal mol}^{-1}$ higher in energy than the most stable isomer **1A** at the B3LYP-D3/aug-cc-pVTZ level, which are unlikely to be observed in the experiments. The calculated

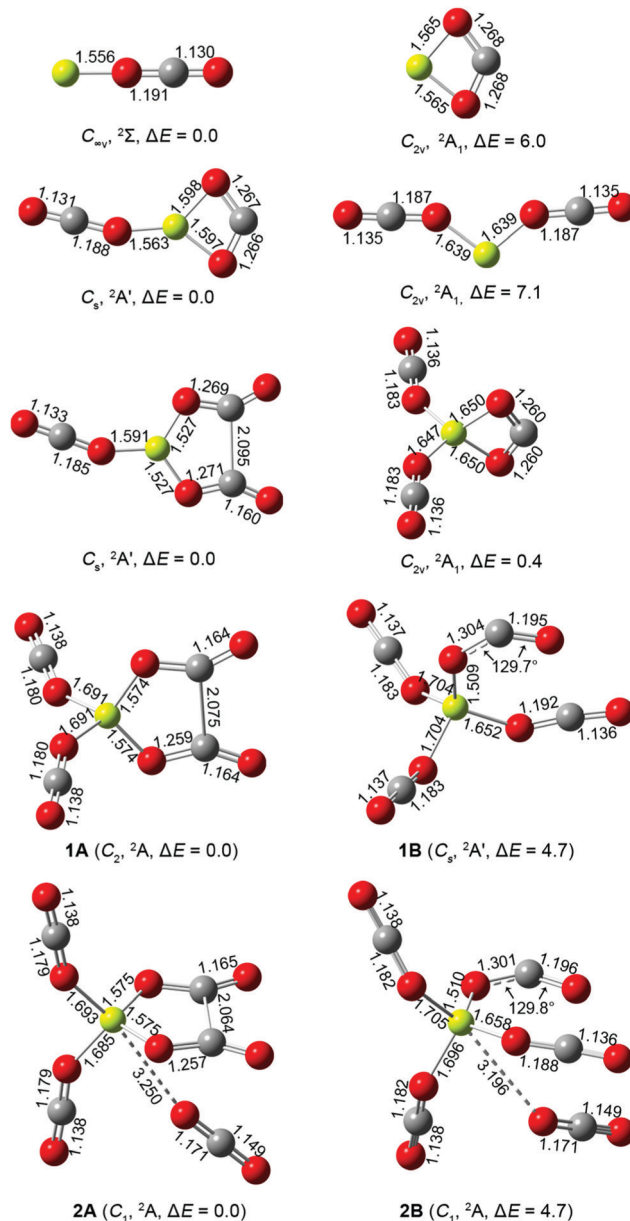


Fig. 3 Optimized structures (bond length in \AA and bond angle in $^\circ$) of the two lowest-lying structural isomers of the $\text{Be}(\text{CO}_2)_n^+$ ($n = 1-5$) complexes at the B3LYP-D3/aug-cc-pVTZ level. The relative stabilities are also given in kcal mol^{-1} .

vibrational frequencies and intensities of these isomers are collected in Table S1 in the ESI.† The simulated infrared spectra of the two lowest-lying isomers of the $\text{Be}(\text{CO}_2)_4^+$ cation complex are compared to the experimental spectrum in Fig. 4. The sum of the two simulated spectra shows good agreement with the experimental spectrum, suggesting that the observed $\text{Be}(\text{CO}_2)_4^+$ cation complex can be assigned to a mixture of isomers **1A** and **1B**.

The broad band centered at 2380 cm^{-1} that is blue shifted by 31 cm^{-1} from the antisymmetric stretching mode of free CO_2 is attributed to the antisymmetric CO_2 stretching vibrations of the η^1 -O end-on bonded CO_2 ligands. The assignment of

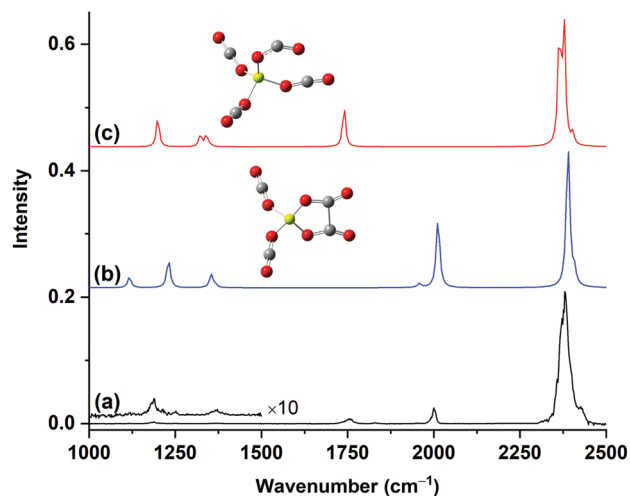


Fig. 4 Experimental infrared spectrum (a) and simulated vibrational spectra (b) and (c) of the $\text{Be}(\text{CO}_2)_4^+$ cation. The simulated spectra were obtained from scaled harmonic frequencies and intensities for the two lowest-lying structural isomers (**1A** and **1B** in Fig. 3) calculated at the B3LYP-D3/aug-cc-pVTZ level.

isomer **1A** is confirmed by the experimental observation of two bands at 2000 and 1950 cm^{-1} , which are due to the antisymmetric and symmetric CO stretching vibrations of the C_2O_4 subunit. These two modes were predicted at 2010 and 1958 cm^{-1} at the B3LYP level (Table 1). The coexistence of isomer **1B** is supported by the experimental observation of the band at 1754 cm^{-1} . This band can be assigned to the antisymmetric CO_2 stretching mode of the bent CO_2 ligand of **1B**, which matches the calculated value of 1740 cm^{-1} very well. Calculations predicted that the other four high-lying isomers (Fig. S1, 1C–1F, ESI†) do not have any vibrations in the 1600–2300 cm^{-1} frequency region (Table S1, ESI†). The comparison of the calculated vibrational frequencies with the experimental values of isomers **1A** and **1B** are listed in Table 1.

The $\text{Be}(\text{CO}_2)_5^+$ complex was also calculated. The two lowest-lying isomers are shown in Fig. 3. Both structures are very weakly bound complexes involving a tagged CO_2 ligand with quite long Be– CO_2 distances (3.250 Å in **2A** and 3.196 Å in **2B**).

Table 1 Comparison between the experimental and calculated (B3LYP-D3/aug-cc-pVTZ) vibrational frequencies of the two structural isomers of $\text{Be}(\text{CO}_2)_4^+$. The calculated frequencies are scaled by a factor of 0.975. The calculated IR intensities are listed in parentheses in km mol^{-1} . The experimental values in parentheses are taken from the spectrum of $\text{Be}(\text{CO}_2)_5^+$

1A		1B	
Exptl	Calcd	Exptl	Calcd
(2404)	2407 (167)	(2404)	2402 (115)
2380	2389 (1639)	2380	2378 (1237)
2000	2010 (798)		2364 (1115)
1950	1958 (45)	1754	1740 (412)
	1365 (31)		1352 (15)
1369	1355 (152)		1340 (122)
1189	1230 (320)	(1296)	1322 (127)
(1088)	1116 (122)	(1202)	1199 (306)

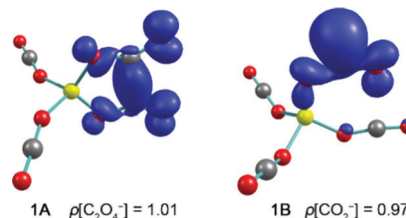


Fig. 5 Calculated spin densities of isomers (**1A** and **1B**) of $\text{Be}(\text{CO}_2)_4^+$ at the B3LYP-D3/aug-cc-pVTZ level. The calculated spin densities are taken from the Mulliken atomic spin densities (in a.u.).

The structures of the $\text{Be}(\text{CO}_2)_4^+$ core ion correlate to the two lowest-lying isomers (**1A** and **1B**) of $\text{Be}(\text{CO}_2)_4^+$. The simulated spectra of these two isomers of $\text{Be}(\text{CO}_2)_5^+$ are compared with the experimental spectrum in Fig. S2 in the ESI.† The results support the conclusion that both **2A** and **2B** isomers were formed in the experiments. It seems that the contribution of isomer **2A** outweighs that of isomer **2B** in the experimental spectrum.

The calculated AIM⁵⁵ charge distributions of the two experimentally observed $\text{Be}(\text{CO}_2)_4^+$ isomers are listed in Table S2 in the ESI.† The results show that the beryllium center has a positive charge of +1.74e in both isomers. The C_2O_4 moiety in **1A** carries a negative charge of $-0.84e$, and thus, it can be described as $\text{Be}^{2+}(\text{C}_2\text{O}_4^-)(\text{OCO})_2$. The bent CO_2 ligand in **1B** carries a negative charge of $-0.83e$. Accordingly, **1B** can be denoted as $\text{Be}^{2+}(\text{CO}_2^-)(\text{OCO})_3$. Fig. 5 shows the calculated spin densities of the two isomers of $\text{Be}(\text{CO}_2)_4^+$. The unpaired electron is nearly exclusively located on the C_2O_4^- moiety in **1A** and on the bent CO_2^- ligand in **1B**.

The small complexes $\text{Be}(\text{CO}_2)_n^+$ ($n = 1-3$) were also observed in the mass spectrum. However, these complexes were either undissociated or dissociated with very low efficiency due to strong binding in the middle IR frequency region. Theoretical calculations were performed on the $\text{Be}(\text{CO}_2)_n^+$ ($n = 1-3$) complexes. The optimized structures are shown in Fig. S3 in the ESI.† The two lowest-lying isomers are shown in Fig. 3. The most stable structure of BeCO_2^+ is linear with the CO_2 ligand η^1 -O end-on bonded to the Be^+ center. This complex has been observed in solid neon matrix with an antisymmetric CO_2 stretching vibration of 2418.9 cm^{-1} , blue-shifted by 71 cm^{-1} from that of free CO_2 .³⁶ This end-on coordinated structure was predicted to be 6.0 kcal mol^{-1} lower in energy than the η^2 -O, O coordinated isomer with C_{2v} symmetry (Fig. S3, ESI†). The most stable structure of $\text{Be}(\text{CO}_2)_2^+$ was predicted to have C_s symmetry involving an η^1 -O coordinated CO_2 ligand and an η^2 -O, O coordinated CO_2 ligand. The structure with both CO_2 ligands being end-on bonded was predicted to be 7.1 kcal mol^{-1} higher in energy than the most stable structure. The structure with a bent end-on bonded CO_2^- ligand is the third most stable isomer, which lies about 10.1 kcal mol^{-1} higher in energy. The oxalate structure involving a C_2O_4^- moiety was predicted to be 17.3 kcal mol^{-1} less stable than the most stable one. The metal oxalate structure becomes the most favored structure for the $\text{Be}(\text{CO}_2)_3^+$ complex. The isomer with an η^2 -O, O side-on

Table 2 EDA-NOCV results of the isomers **1A** and **1B** at the BP86/TZ2P//B3LYP-D3/aug-cc-pVTZ level of theory.^a Energy values are given in kcal mol⁻¹

Fragments	1A Be(CO ₂) ₂ ²⁺ (S) + C ₂ O ₄ ⁻ (D)	1B Be(CO ₂) ₃ ²⁺ (S) + CO ₂ ⁻ (D)
ΔE_{int}	-353.8	-302.7
ΔE_{Pauli}	88.9	82.3
$\Delta E_{\text{elstat}}^b$	-283.6 (64.1%)	-282.7 (73.5%)
ΔE_{orb}	-159.1 (35.9%)	-102.3 (26.5%)
$\Delta E_{\text{orb}(1)}^c$	-45.6 (28.7%)	-42.1 (41.2%)
$\Delta E_{\text{orb}(2)}^c$	-45.6 (28.7%)	-16.1 (15.7%)
$\Delta E_{\text{orb}(3)}^c$	-19.4 (12.2%)	-15.7 (15.3%)
$\Delta E_{\text{orb}(\text{rest})}^c$	-48.5 (30.4%)	-28.4 (27.8%)

^a Fragments are given in singlet (S) or doublet (D) electronic states.

^b The values in parentheses show the contribution to the total attractive interaction ΔE_{elstat} plus ΔE_{orb} . ^c The values in parentheses show the contribution to the total orbital interaction ΔE_{orb} .

coordinated CO₂ ligand and two equivalent η^1 -O end-on coordinated CO₂ ligands is slightly (0.4 kcal mol⁻¹) higher in energy than the first structure. Geometry optimization on the structure with a bent end-on bonded CO₂⁻ ligand converged to the most stable isomer. These calculation results show that addition of CO₂ molecules gradually increases charge transfer and stabilizes the complexes with activated CO₂. At least two CO₂ molecules are needed to induce the electron transfer from the metal center to the ligands. This is very similar to the recent report on Mg(H₂O)_n(CO₂)⁺, where three H₂O molecules are needed to induce charge transfer with the formation of a bent CO₂⁻ moiety.²⁷

Recent investigation on the BeOCO⁺ cation complex indicates that the metal–ligand bonding involves significant covalent character.³⁶ In order to understand the nature of the metal–ligand bonding in the Be(CO₂)₄⁺ complex, the EDA-NOCV method is used to analyze the bonding situation in isomers **1A** and **1B**. According to the aforementioned bonding analysis, we use the fragments [Be(CO₂)₂²⁺] and [C₂O₄⁻] for **1A**, [Be(CO₂)₃²⁺] and bent [CO₂⁻] for **1B** as interacting species. The numerical results calculated at the BP86/TZ2P level using the B3LYP-D3/aug-cc-pVTZ optimized geometries are collected in Table 2. For both isomers, the contribution of the electrostatic attraction ΔE_{elstat} (64.1% in **1A** and 73.5% in **1B**) is larger than the orbital interaction ΔE_{orb} (35.9% in **1A** and 26.5% in **1B**). There are three major components to the total orbital interactions in isomer **1A**, which provide 69.6% of ΔE_{orb} . The first orbital interaction $\Delta E_{\text{orb}(1)}$ comes from the donation of the HOMO–3 of [C₂O₄⁻] to the LUMO of [Be(CO₂)₂²⁺], which is primarily the 2s atomic orbital of beryllium. The second orbital interaction component $\Delta E_{\text{orb}(2)}$ comes from the donation of the HOMO of [C₂O₄⁻] to the LUMO+1 of [Be(CO₂)₂²⁺], which is essentially the 2p atomic orbital of beryllium. These two components have equal contribution of –45.6 kcal mol⁻¹. The third component $\Delta E_{\text{orb}(3)}$ amounts to –19.3 kcal mol⁻¹, which is due to the donation interaction of HOMO–2 of [C₂O₄⁻] to the vacant LUMO+2 of [Be(CO₂)₂²⁺]. In isomer **1B**, there are also three major components that contribute to the covalent interaction, which involve the donation of the highest-lying singly or doubly occupied molecular orbitals of [CO₂⁻] to

the vacant orbitals of the [Be(CO₂)₃²⁺] fragment. The strongest component provides about 41.2% of the total orbital interaction energy. The next two orbital interaction items $\Delta E_{\text{orb}(2)}$ and $\Delta E_{\text{orb}(3)}$ account for 15.7% and 15.3% of ΔE_{orb} , respectively. The remaining orbital term $\Delta E_{\text{orb}(\text{rest})}$ comes mainly from intra-fragment charge polarization of the charged fragments. The pairwise orbital interactions are visualized and identified with the help of the associated deformation densities $\Delta\rho$ shown in Fig. S4 (ESI[†]), which nicely illustrate the charge flow that accompanies the orbital terms. It becomes obvious that the metal–ligand bonding also involves significant covalent character in both the **1A** and **1B** isomers.

Conclusions

The beryllium–carbon dioxide cation complexes Be(CO₂)_n⁺ are produced by a laser vaporization-supersonic expansion ion source in the gas phase. Mass-selected infrared photodissociation spectroscopy in conjunction with theoretical calculations indicates that the Be(CO₂)₄⁺ cation is an electronically coordination saturated complex exhibiting two structural isomers, which are predicted to be very close in energy. The first structure (**1A**) is a metal oxalate complex involving a C₂O₄⁻ moiety and two equivalent η^1 -O end-on coordinated CO₂ ligands. Another isomer (**1B**) involves an η^1 -O end-on coordinated bent CO₂⁻ ligand and three nearly linear η^1 -O end-on coordinated CO₂ ligands. Bonding analyses reveal that the bonding interactions between [Be(CO₂)₂²⁺] and [C₂O₄⁻] in **1A**, [Be(CO₂)₃²⁺] and bent [CO₂⁻] in **1B** both involve significant covalent character.

Conflicts of interest

There are no conflicts to declare.

Acknowledgements

The experimental work was financially supported by the National Natural Science Foundation of China (grant number 21688102).

Notes and references

- 1 A. M. Appel, J. E. Bercaw, A. B. Bocarsly, H. Dobbek, D. L. DuBois, M. Dupuis, J. G. Ferry, E. Fujita, R. Hille, P. J.-A. Kenis, C. A. Kerfeld, R. H. Morris, C. H.-F. Peden, A. R. Portis, S. W. Ragsdale, T. B. Rauchfuss, J. N.-H. Reek, L. C. Seefeldt and R. K. Thauer, *Chem. Rev.*, 2013, **113**, 6621–6658.
- 2 M. Cokoja, C. Bruckmeier, B. Rieger, W. A. Herrmann and F. E. Kühn, *Angew. Chem., Int. Ed.*, 2011, **50**, 8510–8537.
- 3 H. Schwarz, *Coord. Chem. Rev.*, 2017, **334**, 112–123.
- 4 A. Paparo and J. Okuda, *Coord. Chem. Rev.*, 2017, **334**, 136–149.

- 5 I. Castro-Rodriguez, H. Nakai, L. N. Zakharov, A. L. Rheingold and K. Meyer, *Science*, 2004, **305**, 1757–1759.
- 6 L. G. Dodson, M. C. Thompson and J. M. Weber, *Annu. Rev. Phys. Chem.*, 2018, **69**, 231–252.
- 7 J. Mascetti, F. Galan and I. Pápai, *Coord. Chem. Rev.*, 1999, **190–192**, 557–576.
- 8 M. F. Zhou and L. Andrews, *J. Am. Chem. Soc.*, 1998, **120**, 13230–13239.
- 9 M. F. Zhou, Z. J. Zhou, J. Zhuang, Z. H. Li, K. N. Fan, Y. Y. Zhao and X. M. Zheng, *J. Phys. Chem. A*, 2011, **115**, 14361–14369.
- 10 J. Zhuang, Z. H. Li, K. N. Fan and M. F. Zhou, *J. Phys. Chem. A*, 2012, **116**, 3388–3395.
- 11 Q. N. Zhang, M. H. Chen and M. F. Zhou, *J. Phys. Chem. A*, 2014, **118**, 6009–6017.
- 12 B. J. Knurr and J. M. Weber, *J. Phys. Chem. A*, 2014, **118**, 10246–10251.
- 13 B. J. Knurr and J. M. Weber, *J. Phys. Chem. A*, 2013, **117**, 10764–10771.
- 14 B. J. Knurr and J. M. Weber, *J. Am. Chem. Soc.*, 2012, **134**, 18804–18808.
- 15 M. C. Thompson, J. Ramsay and J. M. Weber, *Angew. Chem., Int. Ed.*, 2016, **55**, 15171–15174.
- 16 B. J. Knurr and J. M. Weber, *J. Phys. Chem. A*, 2014, **118**, 4056–4062.
- 17 B. J. Knurr and J. M. Weber, *J. Phys. Chem. A*, 2014, **118**, 8753–8757.
- 18 S. Debnath, X. W. Song, M. R. Fagiani, M. L. Weichman, M. Gao, S. Maeda, T. Taketsugu, W. Schöllkopf, A. Lyalin, D. M. Neumark and K. R. Asmis, *J. Phys. Chem. C*, 2019, **123**, 8439–8446.
- 19 G. B.-S. Miller, T. K. Esser, H. Knorke, S. Gewinner, W. Schöllkopf, N. Heine, K. R. Asmis and E. Uggerud, *Angew. Chem., Int. Ed.*, 2014, **53**, 14407–14410.
- 20 J. S. Jestila, J. K. Denton, E. H. Perez, T. Khuu, E. Aprá, S. S. Xantheas, M. A. Johnson and E. Uggerud, *Phys. Chem. Chem. Phys.*, 2020, **22**, 7460–7473.
- 21 G. Gregoire and M. A. Duncan, *J. Chem. Phys.*, 2002, **117**, 2120–2130.
- 22 R. S. Walters, N. R. Brinkmann, H. F. Schaefer and M. A. Duncan, *J. Phys. Chem. A*, 2003, **107**, 7396–7405.
- 23 N. R. Walker, R. S. Walters and M. A. Duncan, *J. Chem. Phys.*, 2004, **120**, 10037–10045.
- 24 N. R. Walker, R. S. Walters, G. A. Gieves and M. A. Duncan, *J. Chem. Phys.*, 2004, **121**, 10498–10507.
- 25 J. B. Jaeger, T. D. Jaeger, N. R. Brinkmann, H. F. Schaefer and M. A. Duncan, *Can. J. Chem.*, 2004, **82**, 934–946.
- 26 X. P. Xing, G. J. Wang, C. X. Wang and M. F. Zhou, *Chin. J. Chem. Phys.*, 2013, **26**, 687–693.
- 27 E. Barwa, T. F. Pascher, M. Ončák, C. van der Linde and M. K. Beyer, *Angew. Chem., Int. Ed.*, 2020, **59**, 7467–7471.
- 28 A. M. Ricks, A. D. Brathwaite and M. A. Duncan, *J. Phys. Chem. A*, 2013, **117**, 11490–11498.
- 29 F. S. Menges, S. M. Craig, N. Toetsch, A. Bloomfield, S. Ghosh, H. J. Krueger and M. A. Johnson, *Angew. Chem., Int. Ed.*, 2016, **55**, 1282–1285.
- 30 Z. Zhao, X. T. Kong, D. Yang, Q. Q. Yuan, H. Xie, H. J. Fan, J. J. Zhao and L. Jiang, *J. Phys. Chem. A*, 2017, **121**, 3220–3226.
- 31 A. Iskra, A. S. Gentleman, A. Kartouzian, M. J. Kent, A. P. Sharp and S. R. Mackenzie, *J. Phys. Chem. A*, 2017, **121**, 133–140.
- 32 D. Yang, M. Z. Su, H. J. Zheng, Z. Zhao, G. Li, X. T. Kong, H. Xie, H. J. Fan, W. Q. Zhang and L. Jiang, *Chin. J. Chem. Phys.*, 2019, **32**, 223–228.
- 33 D. Yang, X. T. Kong, H. J. Zheng, M. Z. Su, Z. Zhao, H. Xie, H. J. Fan, W. Q. Zhang and L. Jiang, *J. Phys. Chem. A*, 2019, **123**, 3703–3708.
- 34 X. T. Kong, R. L. Shi, C. Wang, H. J. Zheng, T. T. Wang, X. Q. Liang, J. P. Yang, Q. S. Jing, Y. M. Liu, H. Y. Han, Z. Zhao, H. J. Fan, G. Li and H. Xie, *Chem. Phys.*, 2020, **534**, 110755.
- 35 N. Zimmermann, T. M. Bernhardt, J. M. Bakker, R. N. Barnett, U. Landman and S. M. Lang, *J. Phys. Chem. A*, 2020, **124**, 1561–1566.
- 36 X. L. Dong, C. X. Ding, Q. N. Zhang, M. H. Chen, L. L. Zhao, M. F. Zhou and G. Frenking, *J. Am. Chem. Soc.*, 2021, **143**, 14300–14305.
- 37 G. J. Wang, C. X. Chi, X. P. Xing, C. F. Ding and M. F. Zhou, *Sci. China: Chem.*, 2014, **57**, 172–177.
- 38 C. Shang and Z. P. Liu, *J. Chem. Theory Comput.*, 2013, **9**, 1838–1845.
- 39 A. D. Becke, *J. Chem. Phys.*, 1993, **98**, 5648–5652.
- 40 C. T. Lee, W. T. Yang and R. G. Parr, *Phys. Rev. B: Condens. Matter Mater. Phys.*, 1988, **37**, 785–789.
- 41 D. E. Woon and T. H. Dunning, *J. Chem. Phys.*, 1993, **98**, 1358–1371.
- 42 R. A. Kendall, T. H. Dunning and R. J. Harrison, *J. Chem. Phys.*, 1992, **96**, 6796–6806.
- 43 S. Grimme, J. Antony, S. Ehrlich and H. Krieg, *J. Chem. Phys.*, 2010, **132**, 154104.
- 44 K. Raghavachari, G. W. Trucks, J. A. Pople and M. A. Head-Gordon, *Chem. Phys. Lett.*, 1989, **157**, 479–483.
- 45 M. J. Frisch, G. W. Trucks, H. B. Schlegel, G. E. Scuseria, M. A. Robb, G. Cheeseman, J. R. Scalmani, V. Barone, B. Mennucci, G. A. Petersson, H. Nakatsuji, M. Caricato, X. Li, H. P. Hratchian, A. F. Izmaylov, J. Bloino, G. Zheng, J. L. Sonnenberg, M. Hada, M. Ehara, K. Toyota, R. Fukuda, J. Hasegawa, M. Ishida, T. Nakajima, Y. Honda, O. Kitao, H. Nakai, T. Vreven, J. A. Montgomery Jr., J. E. Peralta, F. Ogliaro, M. Bearpark, J. J. Heyd, E. Brothers, K. N. Kudin, V. N. Staroverov, R. Kobayashi, J. Nomand, K. Raghavachari, A. Rendell, J. C. Burant, S. S. Iyengar, J. Tomasi, M. Cossi, N. Rega, J. M. Millam, M. Klene, J. E. Knox, J. B. Cross, V. Bakken, C. Adamo, J. Jaramillo, R. Gomperts, R. E. Stratmann, O. Yazyev, A. J. Austin, R. Cammi, C. Pomelli, J. W. Ochterski, R. L. Martin, K. Morokuma, V. G. Zakrzewski, G. A. Voth, P. Salvador, J. J. Dannenberg, S. Dapprich, A. D. Daniels, O. Farkas, J. B. Foresman, J. V. Ortiz, J. Cioslowski and D. J. Fox, *Gaussian 09, Revision D.01*, Gaussian, Inc., Wallingford CT, 2013.
- 46 M. Mitoraj and A. Michalak, *J. Mol. Model.*, 2008, **14**, 681–687.

- 47 J. P. Perdew, *Phys. Rev. B: Condens. Matter Mater. Phys.*, 1986, **33**, 8822–8824.
- 48 E. Van Lenthe and E. J. Baerends, *J. Comput. Chem.*, 2003, **24**, 1142–1156.
- 49 G. te Velde, F. M. Bickelhaupt, E. J. Baerends, C. Fonseca Guerra, S. J.-A. van Gisbergen, J. G. Snijders and T. Ziegler, *J. Comput. Chem.*, 2001, **22**, 931–967.
- 50 M. F. Zhou and L. Andrews, *J. Chem. Phys.*, 1999, **110**, 6820–6826.
- 51 M. F. Zhou and L. Andrews, *J. Chem. Phys.*, 1999, **110**, 2414–2422.
- 52 W. E. Thompson and M. E. Jacox, *J. Chem. Phys.*, 1999, **111**, 4487–4496.
- 53 K. O. Hartman and I. C. Hisatsune, *J. Chem. Phys.*, 1966, **44**, 1913–1918.
- 54 T. Sommerfeld, H.-D. Meyer and L. S. Cederbaum, *Phys. Chem. Chem. Phys.*, 2004, **6**, 42–45.
- 55 R. F.-W. Bader, *Atoms in Molecules A Quantum Theory*, Clarendon Press, Oxford, 1990.